Accepted Manuscript

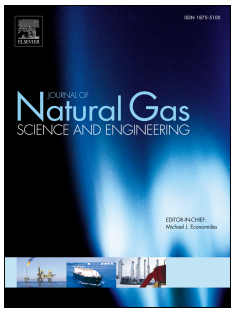

Numerical modeling of isothermal compositional grading by convex splitting methods

Yiteng Li, Jisheng Kou, Shuyu Sun

PII: S1875-5100(17)30139-7

DOI: 10.1016/j.jngse.2017.03.019

Reference: JNGSE 2120

To appear in: *Journal of Natural Gas Science and Engineering*

Received Date: 18 January 2017

Revised Date: 15 March 2017

Accepted Date: 16 March 2017

Please cite this article as: Li, Y., Kou, J., Sun, S., Numerical modeling of isothermal compositional grading by convex splitting methods, *Journal of Natural Gas Science & Engineering* (2017), doi: 10.1016/j.jngse.2017.03.019.

Numerical Modeling of Isothermal Compositional Grading by Convex Splitting Methods

Yiteng Li[1], Jisheng Kou[2], Shuyu Sun[1]

[1]Physical Science and Engineering Division (PSE), King Abdullah University of Science and Technology (KAUST), Thuwal, 23955-6900, Saudi Arabia
[2]School of Mathematics and Statistics, Hubei Engineering University, Xiaogan, 432000, China

Abstract

In this paper, an isothermal compositional grading process is simulated based on convex splitting methods with the Peng-Robinson equation of state. We first present a new form of gravity/chemical equilibrium condition by minimizing the total energy which consists of Helmholtz free energy and gravitational potential energy and incorporating Lagrange multipliers for mass conservation. The time-independent equilibrium equations are transformed into a system of transient equations as our solution strategy. It is proved our time-marching scheme is unconditionally energy stable by the semi-implicit convex splitting method in which the convex parts of Helmholtz free energy and its derivative are treated implicitly and the concave parts are treated explicitly. With relaxation factor controlling Newton iteration, our method is able to converge to a solution with satisfactory accuracy if a good initial estimate of mole compositions is provided. More importantly, it helps us automatically split the unstable single phase into two phases, determine the existence of gas-oil contact (GOC) and locate its position if GOC does exist. A number of numerical examples are presented to show the performance of our method.

Keywords

Isothermal compositional grading; Helmholtz free energy; Convex splitting method; Semi-implicit scheme

1 Introduction

In any comprehensive reservoir study, it is primary to accurately assess the spatial distribution of fluid components, because it plays a significant role in estimation of initial hydrocarbons in place, prediction of gas-oil contact, design of reservoir development plans (Mokhtari and Ashoori, 2013). Further, it also

helps to initializating numerical reservoir simulators for the study of multiphase multicomponent fluid flow where a plenty of research work has been done (Sun and Wheeler, 2005, 2006, 2007). These factors can significantly influence how much hydrocarbons can be produced and what strategy can be used to efficiently recover those hydrocarbons, especially in unconventional reservoirs with geometrical complexity and heterogeneity (Cai et al., 2017). It should be noticed that fluid components do not uniformly distribute in reservoirs due to gravity. As the reservoir height increases, the mole fraction of lighter components is likely to increase while the mole fraction of heavier components is likely to decrease. This leads to fluid properties, such as density, viscosity, bubblepoint/dewpoint pressure, formation volume factor, etc., being functional of depth. This phenomenon is known as compositional grading, which is noticeable in reservoirs that have large thickness and/or the difference between molecular weights of components is substantial.

There are two important compositional grading models, isothermal and non-isothermal. The isothermal model only takes into account the gravitational effect and a gravity/chemical equilibrium condition is established. For the non-isothermal problem, thermal gradient is incorporated into the model. The thermal effect, called thermal diffusion, tends to mitigate gravitational segregation. Namely, lighter components are inclined to move to the high-temperature region which usually locates at the lower part of a reservoir, and heavier components are inclined to move to the low-temperature region. Considering the thermal diffusion coefficient is difficult to measure or estimate, as well as the fact that in some reservoirs the isothermal model fits experimental data or field data much better (Kord and Zobeidi, 2007), we focus on the isothermal compositional grading problem in this paper.

There are a lot of papers about isothermal compositional grading. In 1939, Sage et al. (1939) investigated the influence of gravity effect on the spatial distribution of components in a reservoir fluid system. However, they assumed the fluid mixture behaved like an ideal fluid, which heavily restricted the performance of their method. Later, some works (Schulte, 1980; Whitson and Belery, 1994; Montel et al., 1985) began to focus on more realistic cubic equations of state (EOS), like Peng-Robinson (PR) EOS. Among them, Whitson and Belery (1994) provided an algorithm to analytically solve the isothermal gravity/chemical equilibrium (GCE) problem. However, the phase stability analysis has to be performed to check the stability of gradient solution. This method is classified as the pressure-based method, which means pressure, as well as mole composition, has to be specified at a reference depth. Halldórsson and Stenby (2000) developed a volume-based algorithm for isothermal gravitational segregation afterwards. In 2001, an excellent review about compositional grading (Høier and Whitson, 2001) was published. Mathematical models and corresponding solution algorithms were discussed, and a wide range of reservoir fluid systems were studied. There are also some experimental works (Ratulowski et al., 2000; Ting et al., 2009) performed to investigate the isothermal compositional grading.

In the previous works, it was commonly assumed fluid components have no mass flux, which means all components exist in a stationary state in the ab-

sence of convection. We also follow this assumption in this work. However, this assumption does not mean fluid mixtures are initially at equilibrium. When a multicomponent system reaches the true equilibrium state, the sum of the chemical potential and gravity potential of each component must be constant (Firoozabadi, 2015), yielding a system of non-linear equations. An efficient solution algorithm is successive substitution accelerated with the General Dominant Eigenvalue Method (GDEM) for composition and Newton-Raphson method for pressure (Whitson and Belery, 1994). However, the phase stability analysis is inevitable to verify the validity of gradient solution at each depth. A valid solution indicates a thermodynamically stable single phase. Otherwise, the calculated compositions and pressure will split into two (or more) phases and gradient calculations have to be reinitialized. Obviously, this process has to be repeated and it could take a lot of time to determine solution stability.

In this paper, we present a new form of gravity/chemical equilibrium condition based on the minimizing the total energy which is calculated by integrating the density of Helmholtz free energy and the density of gravitational potential energy over the entire domain. The dynamic model describes the evolutionary process of compositional grading, and meanwhile satisfies the minimum-energy principle which is rigorously proved in the work of Kou and Sun (2017) by applying the thermodynamical laws. In this paper, the energy is minimized directly by the variational principle so that there is no need to solve the partial differential equations, as one advantage of the proposed model. The numerical schemes shall be design to preserve the discrete (free) energy dissipation (Zhonghua Qiao and Shuyu Sun, 2014; Fan et al., 2017; Kou and Sun, 2015; Kou et al., 2016). Under the condition that Helmholtz free energy is decomposed into a convex part and a concave part, this unconditional energy dissipation can be achieved by treating the convex part of Helmholtz free energy implicitly and the concave part explicitly. We incorporate Lagrange multipliers to guarantee mass conservation and utilize relaxation factors to guarantee the positivity of our solution. With a good initial estimate, the semi-implicit convex splitting method is able to converge to the solution with good accuracy. Meanwhile, it automatically yields two phases if the input single phase is unstable at the given condition and helps us determine the location of gas-oil contact if it exits. We need to mention that capillarity is ignored in this work, while it plays an important role for two-phase flow (Kou and Sun, 2016), as well as pseudo-components/components lumping.

The rest of this paper is organized as follows: In section 2, we first derive an equilibrium condition by minimizing the total energy. We will prove energy dissipation with time steps by utilizing the time-dependent gravity/chemical equilibrium equation. In section 3, we split energy functions into convex parts and concave parts. A semi-implicit temporal discretization with Newton-Raphson method is used to solve the system of nonlinear equations for the isothermal compositional grading problem. Details about our solution algorithm are described in this section. In section 4, three numerical examples are presented to show the performance of the proposed method. Finally, we summarize this work and discuss future work.

2 Mathematical model of isothermal fluid system under gravity

According to the second law of thermodynamics, the total energy given by

$$F(\mathbf{n}) = \int_\Omega \left(f_h(\mathbf{n}) + f_g\right) d\mathbf{x} \tag{2.1}$$

should achieve the minimum at the equilibrium state. In (2.1), $f_h(\mathbf{n})$ is the density of Helmholtz free energy and f_g is the density of gravitational potential energy. All details about energy formulations for multicomponent mixture are included in the appendix.

Now we consider the problem of minimizing the total energy:

$$\min F(\mathbf{n}). \tag{2.2}$$

Since the total mole number of each component is conserved, we have the following constraint condition

$$\int_\Omega n_i \, d\mathbf{x} = N_i^t, \quad n_i > 0, \tag{2.3}$$

where N_i^t is the total moles of component i. The constraint condition (2.3) guarantees the mass balance of each component in the domain.

Let

$$\mathcal{C}(\mathbf{n}) = \sum_{i=1}^{N} c_i \left(N_i^t - \int_\Omega n_i \, d\mathbf{x} \right). \tag{2.4}$$

Using the method of Lagrange multipliers, we define the functional

$$\mathcal{L}(\mathbf{n}) = F(\mathbf{n}) + \mathcal{C}(\mathbf{n}). \tag{2.5}$$

Denote $\delta\mathbf{n}_k = (n_1, \ldots, n_{k-1}, n_k + \delta n_k, n_{k+1}, \ldots, n_N)^T$. Consider

$$\begin{aligned} \delta_k F(\mathbf{n}) &= F(\mathbf{n} + \delta n_k \mathbf{e}_k) - F(\mathbf{n}) \\ &= \int_\Omega \left(f_h(\mathbf{n} + \delta\mathbf{n}_k) - f_h(\mathbf{n})\right) d\mathbf{x} + \int_\Omega M_{w,k} g h \delta n_k \, d\mathbf{x} \\ &\simeq \int_\Omega \mu_k^0(\mathbf{n}) \delta n_k \, d\mathbf{x} + \int_\Omega M_{w,k} g h \delta n_k \, d\mathbf{x}. \end{aligned} \tag{2.6}$$

Similarly, we find

$$\delta_k \mathcal{C}(\mathbf{n}) = \mathcal{C}(\mathbf{n} + \delta\mathbf{n}_k) - \mathcal{C}(\mathbf{n}) \simeq -c_k \int_\Omega \delta n_k \, d\mathbf{x}. \tag{2.7}$$

Therefore

$$\begin{aligned} \delta_k \mathcal{L}(\mathbf{n}) &= \delta_k F(\mathbf{n}) + \delta_k \mathcal{C}(\mathbf{n}) \\ &\simeq \int_\Omega (\mu_k(\mathbf{n}) + M_{w,k} g h - c_k) \delta n_k \, d\mathbf{x}. \end{aligned} \tag{2.8}$$

Because δn_k is arbitrary, by the principal of variational calculus (Struwe, 2008), the minimizer of the functional $\mathcal{L}(\cdot)$ satisfies the following equilibrium conditions

$$\mu_i(\mathbf{n}) + M_{w,i} g h - c_i = 0, \quad i = 1, 2, \ldots, N, \tag{2.9}$$

associated with the constraints given in (2.3) where N is the number of components. We can see from (2.9) that at the equilibrium state ($\mu_i + M_{w,i}gh$) shall be constant in the entire domain, and moreover, the molar density distribution shall be inhomogeneous because of the difference of component molecular weights and the variation of height in space.

To apply a time marching scheme, a time-derivative term is added to the left-hand side of (2.9), the gravity/chemical equilibrium equation becomes (Cahn and Allen, 1977)

$$\lambda\frac{\partial n_i}{\partial t} + \mu_i(\mathbf{n}) + M_{w,i}gh - c_i = 0, \quad i = 1, 2, \ldots, N, \tag{2.10}$$

where λ is a coefficient to enforce unit consistency.It can be proved the total energy given by (2.1) decreases with time. Proof procedures are shown below.

Proof: Differentiate (2.1) with respect to time , then we can get

$$\frac{dF(\mathbf{n})}{dt} = \int_\Omega \frac{df_h(\mathbf{n})}{\partial t}\, d\mathbf{x} + \int_\Omega \frac{df_g}{\partial t}\, d\mathbf{x} = \int_\Omega \sum_{i=1}^{N} \mu_i \frac{\partial n_i}{\partial t}\, d\mathbf{x} + \int_\Omega \sum_{i=1}^{N} M_{w,i}gh\frac{\partial n_i}{\partial t}\, d\mathbf{x}.$$

Recall the time-dependent gravity/chemical equilibrium equation (2.10). Substituting μ_i by $\left(c_i - M_{w,i}gh - \lambda\frac{\partial n_i}{\partial t}\right)$, then the above equation can be derived as

$$\begin{aligned}\frac{dF(\mathbf{n})}{dt} &= \int_\Omega \sum_{i=1}^{N} \left(c_i - M_{w,i}gh - \lambda\frac{\partial n_i}{\partial t}\right)\frac{\partial n_i}{\partial t}\, d\mathbf{x} + \int_\Omega \sum_{i=1}^{N} M_{w,i}gh\frac{\partial n_i}{\partial t}\, d\mathbf{x} \\ &= \lambda\int_\Omega \sum_{i=1}^{N} c_i\frac{\partial n_i}{\partial t}\, d\mathbf{x} - \int_\Omega \sum_{i=1}^{N} \left(\frac{\partial n_i}{\partial t}\right)^2 d\mathbf{x}.\end{aligned}$$

According to (2.3), $\lambda\int_\Omega \sum_{i=1}^{N} c_i\frac{\partial n_i}{\partial t}\, d\mathbf{x} = 0$. The derivative of total energy with respect to time is eventually simplified as $-\int_\Omega \sum_{i=1}^{N} \left(\frac{\partial n_i}{\partial t}\right)^2 d\mathbf{x}$, which is always negative. Hereto we have completed the proof.

3 Numerical algorithms

To construct a stable time marching scheme, we first split the density of Helmholtz free energy $f_h(\mathbf{n})$ as the following form

$$f_h(\mathbf{n}) = f_h^{\text{convex}}(\mathbf{n}) + f_h^{\text{concave}}(\mathbf{n}). \tag{3.1}$$

The expressions of μ_k^{convex} and μ_k^{concave} can be derived by calculating derivatives of f_h^{convex} and f_h^{concave} with respect to the molar density of component k, respectively.

$$\mu_k^{\text{convex}}(\mathbf{n}) = \frac{\partial f_h^{\text{convex}}(\mathbf{n})}{\partial n_k} = RT\ln n_k - RT\left(\ln(1-bn) - \frac{nb_k}{1-bn}\right), \tag{3.2}$$

$$\begin{aligned}\mu_k^{\text{concave}}(\mathbf{n}) = \frac{\partial f_h^{\text{concave}}(\mathbf{n})}{\partial n_k} = \frac{2\tilde{a}_k b - ab_k n}{2\sqrt{2}b^2 n}\ln\left(\frac{1+(1-\sqrt{2})bn}{1+(1+\sqrt{2})bn}\right) + \\ \frac{a(T)n}{2\sqrt{2}b}\left(\frac{(1-\sqrt{2})b_k}{1+(1-\sqrt{2})bn} - \frac{(1+\sqrt{2})b_k}{1+(1+\sqrt{2})bn}\right),\end{aligned} \tag{3.3}$$

where

$$\tilde{a}_k = \sum_{j=1}^{N} n_j (a_k a_j)^{1/2} (1 - k_{kj}) \tag{3.4}$$

The derivative of chemical potential, which is the second derivative of Helmholtz free energy density, is given by

$$\frac{\partial \mu_k^{\text{convex}}(\mathbf{n})}{\partial n_l} = RT \left(\delta_{kl} \frac{1}{n_{kl}} + \frac{(b_k + b_l)(1 - bn) + n b_k b_l}{(1 - bn)^2} \right), \tag{3.5}$$

where

$$\delta_{kl} = \begin{cases} 1, & k = l; \\ 0, & k \neq l. \end{cases}$$

Because the equation of $\frac{\partial \mu_k^{\text{concave}}(\mathbf{n})}{\partial n_l}$ is too long, we decompose it into four parts which are shown below:

$$\frac{\partial \mu_k^{\text{concave}}(\mathbf{n})}{\partial n_l} = \frac{1}{2\sqrt{2}} \left(A_1 + A_2 + A_3 + A_4 \right), \tag{3.6}$$

with

$$A_1 = \frac{2 \left(\hat{a}_{kl} bn - \tilde{a}_k b_l - \tilde{a}_l b_k \right) b + 2 a b_k b_l n}{b^3 n^2} \ln \left(\frac{1 + \left(1 - \sqrt{2}\right) bn}{1 + \left(1 + \sqrt{2}\right) bn} \right), \tag{3.7}$$

$$A_2 = \frac{2\tilde{a}_k b - a b_k n}{b^2 n} \left(\frac{\left(1 - \sqrt{2}\right) b_l}{1 + \left(1 - \sqrt{2}\right) bn} - \frac{\left(1 + \sqrt{2}\right) b_l}{1 + \left(1 + \sqrt{2}\right) bn} \right), \tag{3.8}$$

$$A_3 = \frac{2\tilde{a}_l b - a b_l n}{b^2 n} \left(\frac{\left(1 - \sqrt{2}\right) b_k}{1 + \left(1 - \sqrt{2}\right) bn} - \frac{\left(1 + \sqrt{2}\right) b_k}{1 + \left(1 + \sqrt{2}\right) bn} \right), \tag{3.9}$$

$$A_4 = \frac{a(T)\, n}{b} \left(\frac{\left(1 + \sqrt{2}\right)^2 b_k b_l}{\left[1 + \left(1 + \sqrt{2}\right) bn\right]^2} - \frac{\left(1 - \sqrt{2}\right)^2 b_k b_l}{\left[1 + \left(1 - \sqrt{2}\right) bn\right]^2} \right), \tag{3.10}$$

where

$$\hat{a}_{kl} = (a_k a_l)^{1/2} (1 - k_{kl}). \tag{3.11}$$

By treating $\mu_i^{\text{convex}}(\mathbf{n})$ implicitly and $\mu_i^{\text{convcave}}(\mathbf{n})$ explicitly, at kth time step (2.10) can be temporally discretized as

$$\lambda \frac{n_i^{k+1} - n_i^k}{t^{k+1} - t^k} + \mu_i^{\text{convex}}(\mathbf{n}^{k+1}) + \mu_i^{\text{concave}}(\mathbf{n}^k) + M_{w,i} g h - c_i^{k+1} = 0. \tag{3.12}$$

To demonstrate the semi-discrete scheme is unconditionally energy stable, it is assumed the following inequality is satisfied under a certain condition f_h^{convex} is convex and f_h^{concave} is indeed concave (Kou and Sun, 2017)

$$\begin{aligned} f_h(\mathbf{n}^{k+1}) - f_h(\mathbf{n}^k) \leq & \sum_{i=1}^{N} \mu_i^{\text{convex}}(\mathbf{n}^{k+1}) \left(n_i^{k+1} - n_i^k \right) + \\ & \sum_{i=1}^{N} \mu_i^{\text{concave}}(\mathbf{n}^k) \left(n_i^{k+1} - n_i^k \right) \end{aligned} \tag{3.13}$$

By multiplying $\left(n_i^{k+1}-n_i^k\right)$ on the both sides of (3.12), the summation of (3.12) over all components is

$$\begin{aligned}0=&\sum_{i=1}^{N}\lambda\frac{\left(n_i^{k+1}-n_i^k\right)^2}{\Delta t}+\sum_{i=1}^{N}\mu_i^{\text{convex}}(\mathbf{n}^{k+1})\left(n_i^{k+1}-n_i^k\right)+\\&\sum_{i=1}^{N}\mu_i^{\text{concave}}(\mathbf{n}^{k})\left(n_i^{k+1}-n_i^k\right)+\sum_{i=1}^{N}M_{w,i}gh\left(n_i^{k+1}-n_i^k\right)-\\&\sum_{i=1}^{N}c_i^{k+1}\left(n_i^{k+1}-n_i^k\right)\end{aligned}\tag{3.14}$$

Now adding $\left(f_h(\mathbf{n}^{k+1})-f_h(\mathbf{n}^k)\right)$ on the both sides of the above equation, we can derive

$$\begin{aligned}&f_h(\mathbf{n}^{k+1})-f_h(\mathbf{n}^k)-\sum_{i=1}^{N}\mu_i^{\text{convex}}(\mathbf{n}^{k+1})\left(n_i^{k+1}-n_i^k\right)-\\&\sum_{i=1}^{N}\mu_i^{\text{concave}}(\mathbf{n}^{k})\left(n_i^{k+1}-n_i^k\right)=\sum_{i=1}^{N}\lambda\frac{\left(n_i^{k+1}-n_i^k\right)^2}{\Delta t}+f_h(\mathbf{n}^{k+1})-\\&f_h(\mathbf{n}^k)+\sum_{i=1}^{N}M_{w,i}gh\left(n_i^{k+1}-n_i^k\right)-\sum_{i=1}^{N}c_i^{k+1}\left(n_i^{k+1}-n_i^k\right)\end{aligned}\tag{3.15}$$

Considering (3.13), the above equation satisfies the following inequality

$$\begin{aligned}&\left(f_h(\mathbf{n}^{k+1})+m^{k+1}gh\right)-\left(f_h(\mathbf{n}^k)+m^kgh\right)-\sum_{i=1}^{N}c_i^{k+1}\left(n_i^{k+1}-n_i^k\right)\\&\qquad\leq-\sum_{i=1}^{N}\lambda\frac{\left(n_i^{k+1}-n_i^k\right)^2}{\Delta t}\end{aligned}\tag{3.16}$$

Integrating (3.16) over the the entire domain, it becomes

$$\begin{aligned}&\int_\Omega\left(f_h(\mathbf{n}^{k+1})+m^{k+1}gh\right)d\mathbf{x}-\int_\Omega\left(f_h(\mathbf{n}^k)+m^kgh\right)d\mathbf{x}-\\&\int_\Omega\sum_{i=1}^{N}c_i^{k+1}\left(n_i^{k+1}-n_i^k\right)d\mathbf{x}\leq 0\end{aligned}\tag{3.17}$$

Recall the constraint equation (2.3), $\int_\Omega\sum_{i=1}^{N}c_i^{k+1}\left(n_i^{k+1}-n_i^k\right)d\mathbf{x}=0$. Thus,

$$F(\mathbf{n}^{k+1})\leq F(\mathbf{n}^k)\tag{3.18}$$

for any time step size $\Delta t>0$.

In order to highlight the unconditional energy decay of the semi-implicit convex splitting method, we also provide a brief derivation to show the upper limit of Δt for fully implicit and fully explicit scheme. For fully implicit scheme, (3.12) becomes

$$\lambda\frac{n_i^{k+1}-n_i^k}{t^{k+1}-t^k}+\mu_i^{\text{convex}}(\mathbf{n}^{k+1})+\mu_i^{\text{concave}}(\mathbf{n}^{k+1})+M_{w,i}gh-c_i^{k+1}=0.$$

According to the Taylor expansion, the concave part of Helmholtz free energy satisfies the following inequality

$$f_h^{\text{concave}}(\mathbf{n}^{k+1}) - f_h^{\text{concave}}(\mathbf{n}^k) \geq \sum_{i=1}^{N} \mu_i^{\text{concave}}(\mathbf{n}^{k+1}) \left(n_i^{k+1} - n_i^k\right)$$

Now we have

$$f_h(\mathbf{n}^{k+1}) - f_h(\mathbf{n}^k) + \sum_{i=1}^{N} M_{w,i} g h \left(n_i^{k+1} - n_i^k\right) - \sum_{i=1}^{N} c_i^{k+1} \left(n_i^{k+1} - n_i^k\right) \leq$$
$$-\sum_{i=1}^{N} \lambda \frac{\left(n_i^{k+1} - n_i^k\right)^2}{\Delta t} + f_h^{\text{concave}}(\mathbf{n}^{k+1}) - f_h^{\text{concave}}(\mathbf{n}^k) - \sum_{i=1}^{N} \mu_i^{\text{concave}}(\mathbf{n}^k) \left(n_i^{k+1} - n_i^k\right)$$

Integrating the above inequality over the entire domain, it becomes

$$F(\mathbf{n}^{k+1}) - F(\mathbf{n}^k) \leq$$
$$\int_\Omega \left(f_h^{\text{concave}}(\mathbf{n}^{k+1}) - f_h^{\text{concave}}(\mathbf{n}^k) - \sum_{i=1}^{N} \mu_i^{\text{concave}}(\mathbf{n}^k) \left(n_i^{k+1} - n_i^k\right) \right) d\mathbf{x} -$$
$$\int_\Omega \sum_{i=1}^{N} \lambda \frac{\left(n_i^{k+1} - n_i^k\right)^2}{\Delta t} d\mathbf{x}$$

To guarantee energy dissipation, the right-hand side of should be no greater than zero, which means

$$\int_\Omega \sum_{i=1}^{N} \lambda \frac{\left(n_i^{k+1} - n_i^k\right)^2}{\Delta t} d\mathbf{x} \geq$$
$$\int_\Omega \left(f_h^{\text{concave}}(\mathbf{n}^{k+1}) - f_h^{\text{concave}}(\mathbf{n}^k) - \sum_{i=1}^{N} \mu_i^{\text{concave}}(\mathbf{n}^k) \left(n_i^{k+1} - n_i^k\right) \right) d\mathbf{x}$$

Recall the local inequality $f_h^{\text{concave}}(\mathbf{n}^{k+1}) - f_h^{\text{concave}}(\mathbf{n}^k) \geq \sum_{i=1}^{N} \mu_i^{\text{concave}}(\mathbf{n}^{k+1}) \left(n_i^{k+1} - n_i^k\right)$. Considering the integral of the above inequality is greater than zero over the entire domain, we can derive $F(\mathbf{n}^{k+1}) \leq F(\mathbf{n}^k)$ at

$$\Delta t \leq \frac{\int_\Omega \sum_{i=1}^{N} \lambda \left(n_i^{k+1} - n_i^k\right)^2 d\mathbf{x}}{\int_\Omega \left(f_h^{\text{concave}}(\mathbf{n}^{k+1}) - f_h^{\text{concave}}(\mathbf{n}^k) - \sum_{i=1}^{N} \mu_i^{\text{concave}}(\mathbf{n}^{k+1}) \left(n_i^{k+1} - n_i^k\right) \right) d\mathbf{x}}$$

Similarly, for fully explicit scheme, (3.12) becomes

$$\lambda \frac{n_i^{k+1} - n_i^k}{t^{k+1} - t^k} + \mu_i^{\text{convex}}(\mathbf{n}^k) + \mu_i^{\text{concave}}(\mathbf{n}^k) + M_{w,i} g h - c_i^{k+1} = 0.$$

According to the Taylor expansion, the convex part of Helmholtz free energy satisfies the following inequality

$$f_h^{\text{convex}}(\mathbf{n}^{k+1}) - f_h^{\text{convex}}(\mathbf{n}^k) \geq \sum_{i=1}^{N} \mu_i^{\text{convex}}(\mathbf{n}^k) \left(n_i^{k+1} - n_i^k\right)$$

Following the similar derivation procedures for fully implicit scheme and satisfying the following inequality

$$\int_\Omega \left(f_h^{\text{convex}}(\mathbf{n}^{k+1}) - f_h^{\text{convex}}(\mathbf{n}^k) - \sum_{i=1}^N \mu_i^{\text{convex}}(\mathbf{n}^k) \left(n_i^{k+1} - n_i^k\right) \right) d\mathbf{x} > 0,$$

we can get $F(\mathbf{n}^{k+1}) \leq F(\mathbf{n}^k)$ at

$$\Delta t \leq \frac{\int_\Omega \sum_{i=1}^N \lambda \left(n_i^{k+1} - n_i^k\right)^2 d\mathbf{x}}{\int_\Omega \left(f_h^{\text{convex}}(\mathbf{n}^{k+1}) - f_h^{\text{convex}}(\mathbf{n}^k) - \sum_{i=1}^N \mu_i^{\text{convex}}(\mathbf{n}^k) \left(n_i^{k+1} - n_i^k\right) \right) d\mathbf{x}}$$

In (3.12), the unknowns are molar density $\mathbf{n} = (n_1, n_2, \ldots, n_N)^T$ and Lagrange multiplier $\mathbf{c} = (c_1, c_2, \ldots, c_N)^T$. If the domain height is divided into M, the total number of unknowns is $N(M+1)$. Apart from $N \times M$ nonlinear equilibrium equations given by (3.12), N mass constraint equations are needed to uniquely determine all the unknowns, which are shown as below

$$\sum_{j=1}^M h_j n_{i,j}^{k+1} - N_i^t = 0, \quad i = 1, 2, \ldots, N, \tag{3.19}$$

where h_j is the height of jth interval and $n_{i,j}$ is the molar density of component i in jth interval.

In this work, we equally divide the domain height for simplicity. The Newton-Raphson method is applied to solve nonlinear equations. To make sure all molar densities are positive, relaxation factor is added in our code to control the Newton step size. Once the relaxation factor is invoked, it continuously doubles until molar density is nonnegative. Only the convex part of chemical potential and its derivative need to be updated in each newton iteration. Once inner iteration stops, the total energy at the current time step and the relative residual of the total energy between two neighboring time steps is calculated and collected until the predefined tolerance is reached.

It should be mentioned we also test both fully explicit and fully implicit time schemes (not shown in this paper). For the fully explicit scheme, numerical results indicate the time step Δt should be small enough for the solution convergence. A binary mixture of methane and n-pentane at ambient temperature is tested with initial molar density being 500 mol/m^3, respectively. In that case, the solution will be reached only if $\Delta t \leq 0.1$. When the difference between molecular weights increases, for example, a binary mixture of methane and n-decane under the same condition, it fails to converge to the solution with $\Delta t = 10^{-12}$. Interestingly, the fully implicit scheme does not work well either. As shown by our proof, if the time step size is larger than expected, total energy will never decrease. We find the maximum time step $\Delta t_{\max} \approx 0.1$ for solution convergence if we employ the fully implicit scheme in the synthetic oil case. Again, to make sure energy decay with time steps, the convex part must be treated implicitly and the concave part must be treated explicitly. This, in turn, demonstrates the validity of our splitting scheme mentioned at the beginning of this section.

4 Numerical results

In this section, we first verify the validity of the semi-implicit convex splitting method and then test three examples to show the performance of our method. For the last three examples, the domain height is set to 100 m and the number of height intervals is 100. The tolerances for both energy dissipation and newton iteration are 10^{-8}. Since our time marching scheme is unconditionally stable, the size of time step could be very large. Here we set $\Delta t = 10^5$ in this work.

4.1 Model verification

4.1.1 Example 1: Acid gas

This example is used to verify our model by comparing our numerical results with molecular dynamics(MD) results calculated by Galliero and Montel (Galliero et al., 2009). The acid gas mixture consists of methane(C_1), carbon dioxide(CO_2) and hydrogen sulfide(H_2S) whose average mole fraction is 0.28, 0.71 and 0.01, respectively. The thickness of the vertical gas column is 1600 m, and the pressure and temperature at the reference depth is 40 MPa and 443.15 Kelvin.

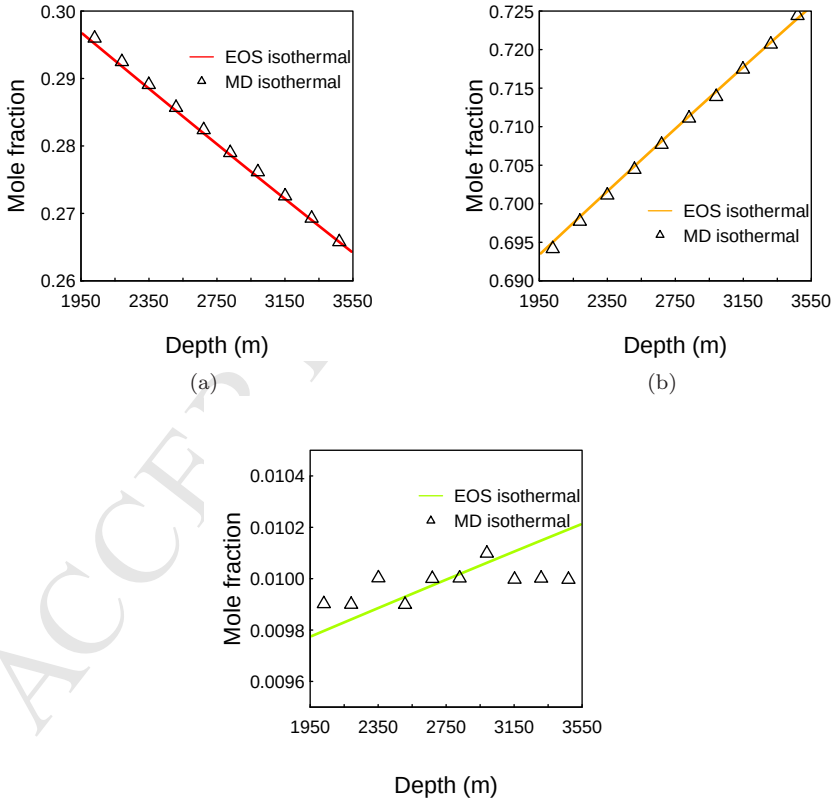

Figure 1: Mole fraction distribution: (a) C_1, (b) CO_2 and (c) H_2S along depth at 443.15 Kelvin

To fit the MD results much better, we first calculate the total molar density of the gas mixture by PR EOS. The total molar density at the reference pressure and temperature is approximately 11000 mol/m^3. Figure 1 shows the compositional variance of acid gas mixture along depth. Apparently, our numerical results fit the MD data very well, especially for C_1 and CO_2. Even though we do not use the initial estimate of the total molar density given by PR EOS, the relative error is acceptable. It's approximately 1.2% when the total molar density is 1000 mol/m^3.

4.1.2 Example 2: Real reservoir fluid

To verify the applicability of the semi-implicit convex splitting method further, we use a test case proposed by Montel et al. (1985). In this case, the reservoir fluid consists of a condensate gas and a light oil. No GOC is found between the vapor and liquid phase. Table 1-3 presents the compositional grading of the field data and the authors' work, gas composition with physical properties at reference depth and binary interaction coefficients, respectively.

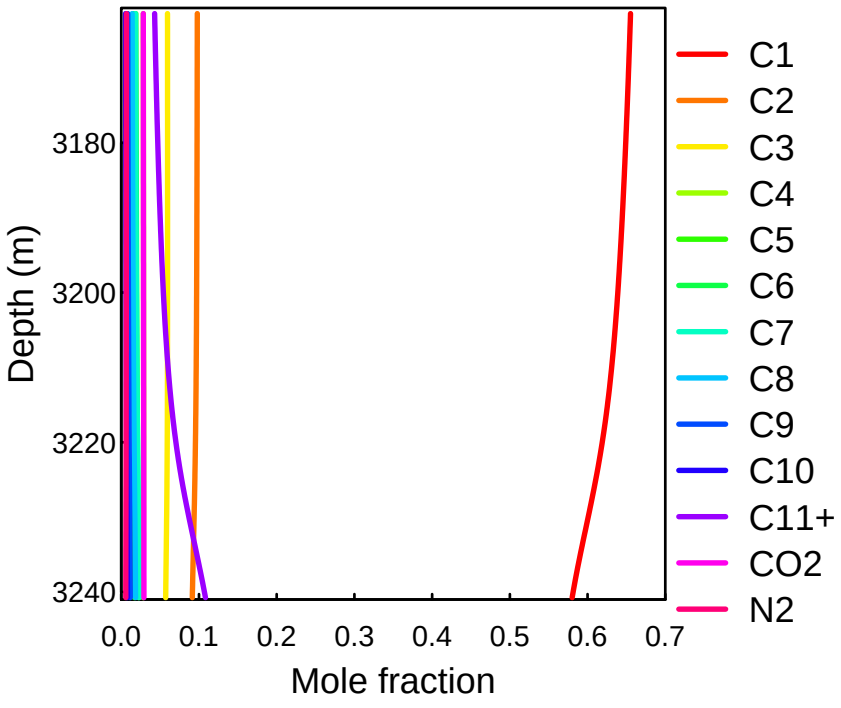

Figure 2: Compositional variance of the real reservoir fluid at 379.8 Kelvin

Figure 2 shows the mole fraction distributions of all thirteen components with depth. It can be seen a phase change occurs at the lower part of the system and there is no apparent interface between two phases. This matches with the fact that no gas-oil contact is found between the condensate gas and the light oil. By comparing our numerical results with the experimental data, our methods

shows good accuracy. At the reference depth, only C_{11+} shows relatively large deviation, approximately 20%, from its experimental data. Comparing to the calculated results given by the authors, our numerical result is closer to the experimental data at 3241 m but shows a larger deviation than the authors' work at 3204.5 m. The deviations result from a few reasons. First, there is a small positive temperature gradient from the reference depth to the "bottom" depth (3241 m). In other words, the temperature at the "bottom" depth is slightly higher than that at the reference depth. Considering the thermal effect tends to mitigate gravitational segregation, our solution should be less accurate in the middle. In addition, the reservoir thickness is 134 m, but we consider the thickness between the reference and the "bottom" depth as our target domain because the exact top and bottom depth are not given. The truncated thickness reduces the gravitational effect on the fluid in the middle of fluid column, causing our numerical results deviating from the experimental data. However, under this situation, our model is still able to capture the compositional grading at the "top" and "bottom".

Table 1: Composition grading with depth

Constituent	3179.5 m*	3204.5 m		3241 m	
	Experimental	Experimental	Calculated	Experimental	Calculated
C_1	63.14	57.20	61.43	53.06	58.27
C_2	9.62	9.53	9.48	9.84	9.13
C_3	5.92	6.33	5.86	6.65	5.68
C_4	2.86	3.24	2.86	3.49	2.80
C_5	1.67	2.01	1.67	2.25	1.65
C_6	2.01	2.51	2.09	2.88	2.18
C_7	1.99	2.50	2.11	2.93	2.26
C_8	1.56	1.98	1.68	2.31	1.82
C_9	0.95	1.61	1.02	1.39	1.12
C_{10}	0.64	0.78	0.68	0.95	0.76
C_{11+}	6.13	9.02	7.62	11.00	10.83
CO_2	2.87	2.75	2.89	2.75	2.91
N_2	0.64	0.54	0.62	0.51	0.59

* Reference.

Table 2: Gas composition with physical properties at reference depth

Component	Mole Fraction	M_w (g/mol)	T_c (K)	P_c (MPa)	ω
C_1*	0.6314	16.04	190.60	4.600	0.0115
C_2*	0.0962	30.07	305.40	4.884	0.0908
C_3*	0.0592	44.10	369.80	4.246	0.1454
C_4	0.0286	58.12	421.09	3.769	0.1886
C_5	0.0167	72.06	467.85	3.424	0.2257
C_6	0.0201	84.43	521.99	3.466	0.2564
C_7	0.0199	97.58	557.09	3.262	0.2854
C_8	0.0166	111.39	585.98	2.889	0.3216
C_9	0.0095	125.94	608.03	2.599	0.3792
C_{10}	0.0064	141.58	620.67	2.306	0.4101
C_{11+}	0.0613	242.75	693.15	1.700	0.7000
CO_2*	0.0287	44.01	304.20	7.376	0.2250
N_2*	0.0064	28.01	126.20	3.394	0.0400

* Pure component.

Table 3: Binary interaction coefficients

	C_1	C_2	C_3	C_4	C_5	C_6	C_7	C_8	C_9	C_{10}	C_{11+}	CO_2	N_2
C_1	0.000	0.000	0.000	0.016	0.022	0.045	0.045	0.045	0.060	0.080	0.140	0.000	0.120
C_2	0.000	0.000	0.000	0.010	0.010	0.010	0.010	0.010	0.060	0.080	0.132	0.000	0.120
C_3	0.000	0.000	0.000	0.010	0.010	0.010	0.010	0.010	0.010	0.010	0.130	0.000	0.120
C_4	0.016	0.010	0.010	0.000	0.000	0.000	0.000	0.000	0.000	0.000	0.125	0.000	0.120
C_5	0.022	0.010	0.010	0.000	0.000	0.000	0.000	0.000	0.000	0.000	0.120	0.000	0.120
C_6	0.045	0.010	0.010	0.000	0.000	0.000	0.000	0.000	0.000	0.000	0.080	0.000	0.120
C_7	0.045	0.010	0.010	0.000	0.000	0.000	0.000	0.000	0.000	0.000	0.060	0.000	0.120
C_8	0.045	0.010	0.010	0.000	0.000	0.000	0.000	0.000	0.000	0.000	0.060	0.000	0.120
C_9	0.060	0.060	0.010	0.000	0.000	0.000	0.000	0.000	0.000	0.000	0.060	0.000	0.120
C_{10}	0.080	0.080	0.010	0.000	0.000	0.000,	0.000	0.000	0.000	0.000	0.060	0.000	0.120
C_{11+}	0.140	0.132	0.130	0.125	0.120	0.080	0.060	0.060	0.060	0.060	0.000	0.000	0.120
CO_2	0.000	0.000	0.000	0.000	0.000	0.000	0.000	0.000	0.000	0.000	0.000	0.000	0.000
N_2	0.120	0.120	0.120	0.120	0.120	0.120	0.120	0.120	0.120	0.120	0.120	0.000	0.000

4.2 Model Prediction

4.2.1 Example 1: C_1-CO_2 mixture

In this example, we first test the influence of temperature on the distribution of a binary mixture of C_1 and CO_2). Initially, we assume the molar density of C_1 to CO_2 is equal. Figure 3 shows the predicted C_1 and CO_2 variation with height at 6 different temperatures. The total molar density is 1000 mol/m^3 (left column) and 5000 mol/m^3 (mid column) and 10000 mol/m^3 (right column), respectively.

As shown in Figure 3, it is clear that methane moves upwards to the top while carbon dioxide prefers to segregate at the bottom because of its larger molecular weight. The maximum compositional variance is found at 338.15 K.Figure 3g-3i

shows the gravitational segregation is mitigated by thermal effect because the mole fraction ratio has smaller slope as temperature increases. It also can be seen the total molar density has limited influence on spatial distribution of C_1 and CO_2 vertically. With temperature increasing, the effect of the total molar density is less significant.

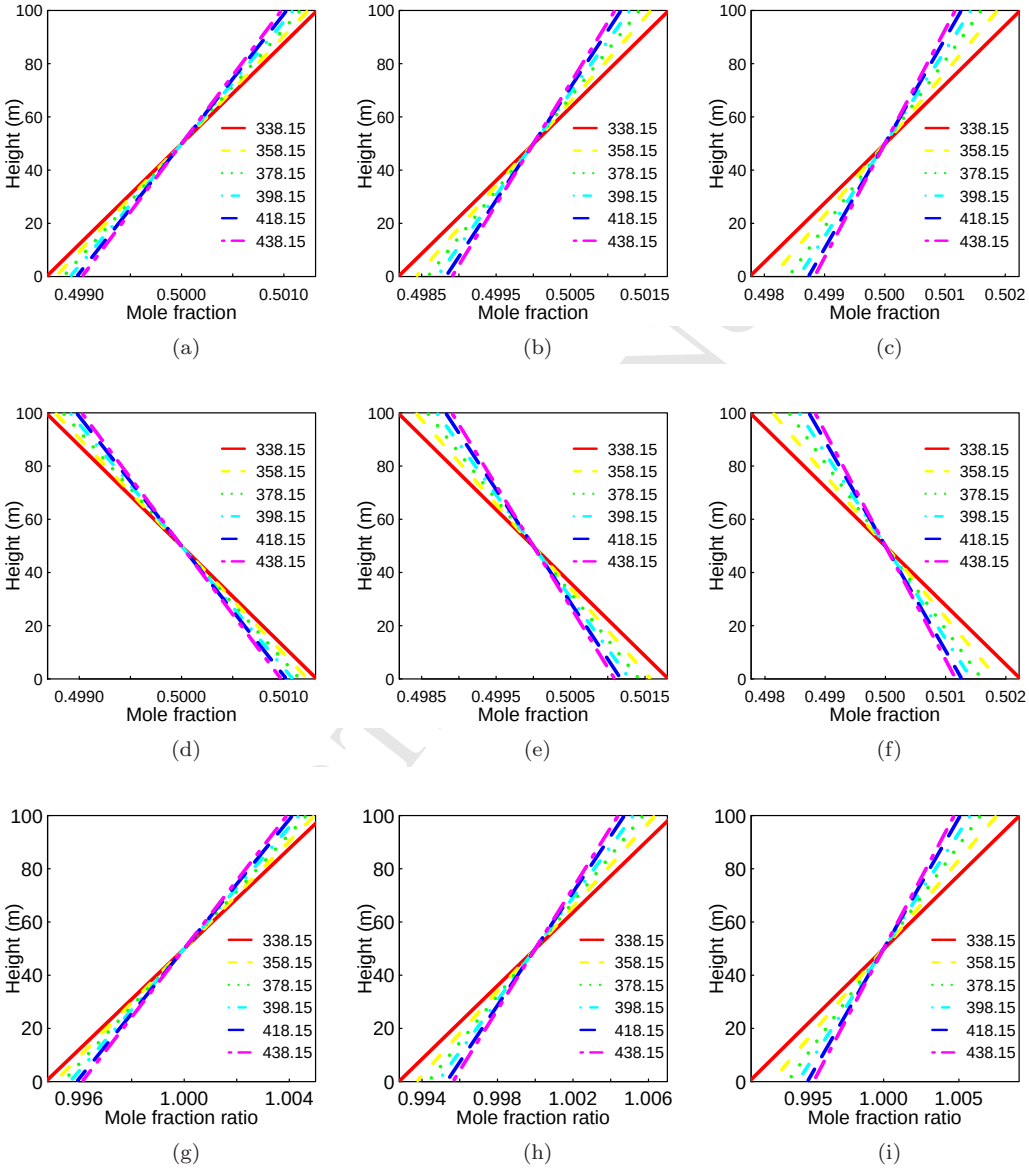

Figure 3: Mole fractions of C_1 (top row), CO_2 (mid row) and their mole fraction ratio (bottom row) at different temperatures. From left to right, the total molar density is 1000 mol/m^3 (left column), 5000 mol/m^3 and 10000 mol/m^3, respectively.

This example is instructive for enhancing methane recovery by CO_2 flooding. As CO_2 is injected, it gradually tends to flow along the lower part of reservoirs under gravity. As a result, the recovery efficiency of CO_2 injection is not as high as expected. One possible method to enhance methane production as expected is injecting high-temperature CO_2 so that the gravitational segregation of CO_2 could be weakened.

4.2.2 Example 2: Simplified natural gas

In this example, we consider a simplified natural gas mixture. The natural gas composition is published by Union Gas Limited. (2017). We simplify the real composition of natural as a gas mixture of C_1, C_2, C_3, CO_2 and N_2. These are the first five components based on the amount of mole fraction. In order to make the total mole fraction equal to 1, we add the sum of mole fractions of all the rest components to the mole fraction of CO_2. Therefore, the mole fraction of C_1, C_2, C_3, CO_2 and N_2 is 0.95, 0.032, 0.002, 0.006 and 0.01, respectively.

Figure 4, 5 and 6 show the compositional variance of the simplified natural gas mixture along height at different temperatures. Each figure corresponds to a different total molar density. It is clear methane tends to move upwards while all the other components tend to move downwards. In general, the gravitational segregation is gradually mitigated as temperature increases. It also can bee seen the compositional grading is not much sensitive to the temperature when temperature is higher than 448.15 Kelvin. Interestingly, when the total molar density is equal to 5000 mol/m^3, we observe nitrogen first suffers more gravitational segregation when temperature increases to 348.15 K. As temperature goes higher, the gravity effect is mitigated. It should be noticed that the total molar density aggravate the compositional segregation at the ambient temperature. When temperature is lower than 348.15 K, the total molar density reduce the effect of thermal diffusion. Above 348.15 K, the effect of mole amount and the thermal effect seems to balance each other but the latter plays a little bigger role. As a result, the mole fraction change of N_2 is restricted to very small scales, as shown in Figure 4e-6e. In this process, the maximum difference is 0.021%.

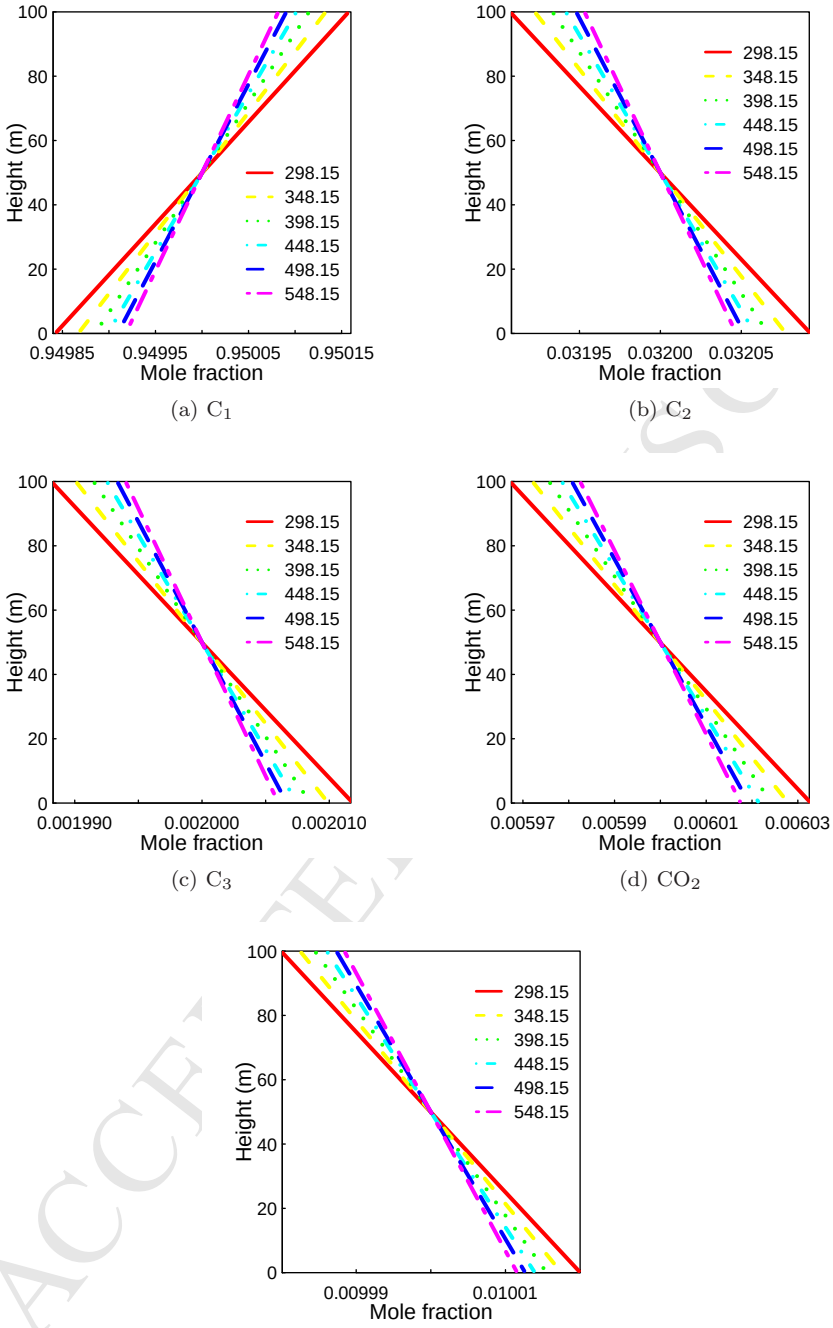

(a) C_1 (b) C_2

(c) C_3 (d) CO_2

(e) N_2

Figure 4: Compositional grading of simplified natural gas when the total molar density is 1000 mol/m^3

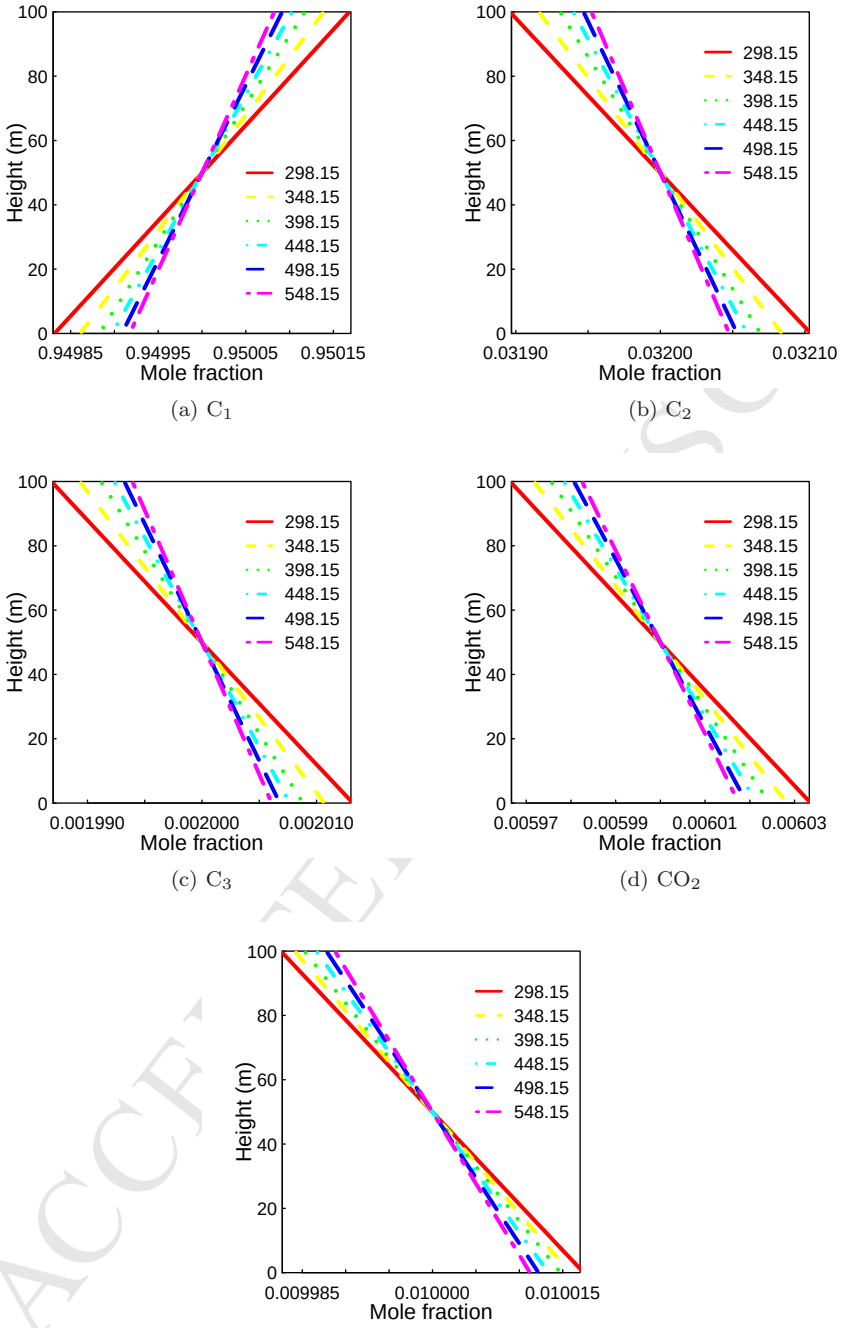

(a) C_1 (b) C_2

(c) C_3 (d) CO_2

(e) N_2

Figure 5: Compositional grading of simplified natural gas when the total molar density is 2000 mol/m^3

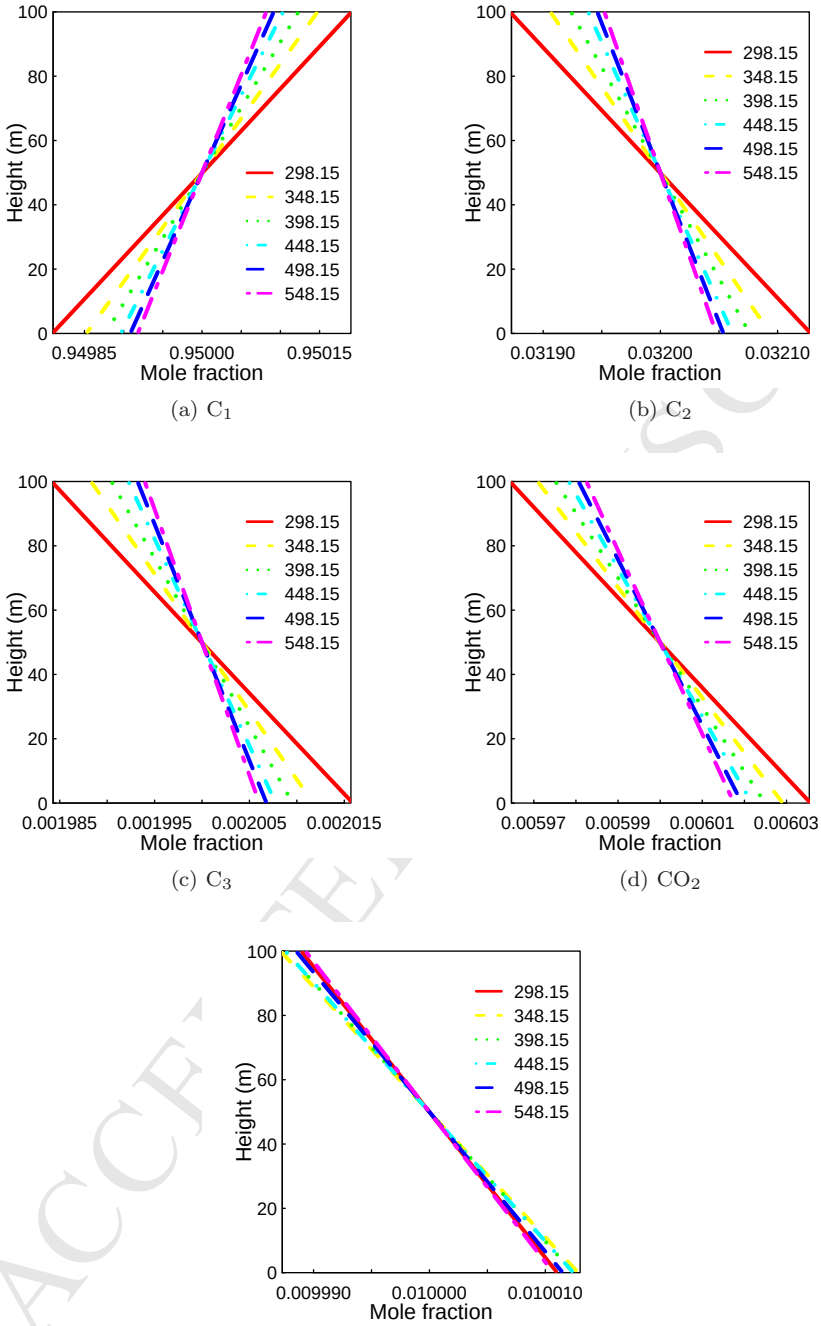

(a) C_1 (b) C_2

(c) C_3 (d) CO_2

(e) N_2

Figure 6: Compositional grading of simplified natural gas when the total molar density is 5000 mol/m^3

4.2.3 Example 3: Synthetic oil

This example is used to show the capability of our method to simulate the isothermal compositional grading of two phases with gas-oil contact. The fluid mixture is composed of methane(C_1), ethane(C_2), propane(C_3), n-pentane(nC_5), n-heptane(nC_7) and n-decane(nC_{10}). We call it synthetic oil, although its composition is far from the real oil composition. Initially ,we assume the fluid mixture is in vapor phase. The system temperature is 378.15 K and the molar density of each component is 500 mol/m^3.

Figure 7 shows the mole fraction distribution of all six components with depth. We find the fluid mixture is automatically split in two phases and a sharp interface exists between vapor and liquid phase because capillarity is ignored in this work. It is clear that lighter components, C_1, C_2 and C_3, have higher mole fraction in the vapor phase and heavier components, nC_5, nC_7 and nC_{10}, have higher mole fraction in the liquid phase.

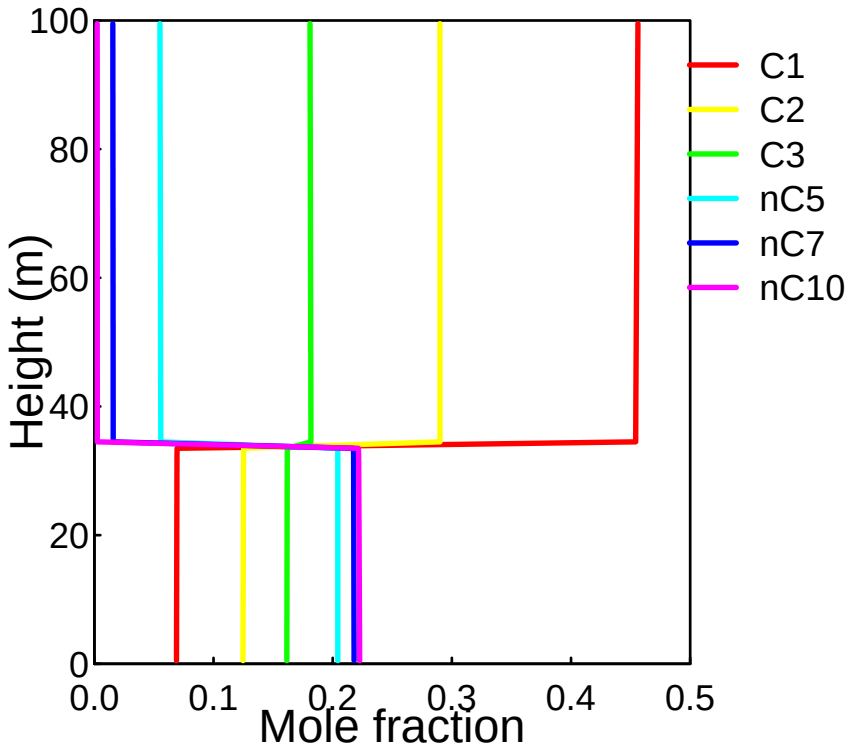

Figure 7: Mole fraction distribution of C_1, C_2, C_3, nC_5, nC_7 and nC_{10} at 378.15 K.

In order to see more details in both phases, Figure 7 is separated based on the vapor-liquid interface and Figure 8 and 9 are generated. Figure 8 and 9 show compositional gradients of all six components in the vapor and liquid phase, re-

spectively. we find all the heavier components except methane move downwards in the vapor phase while only nC_5, nC_7 and nC_{10} tend to move downwards in the liquid phase. This might result from heavy components being inclined to stay in the liquid phase while light components inclined to escape to the vapor phase from the liquid phase. Large molecular weight aggravates gravitational segregation. Therefore, mole fraction of heavier components follow the order of their molecular weights.

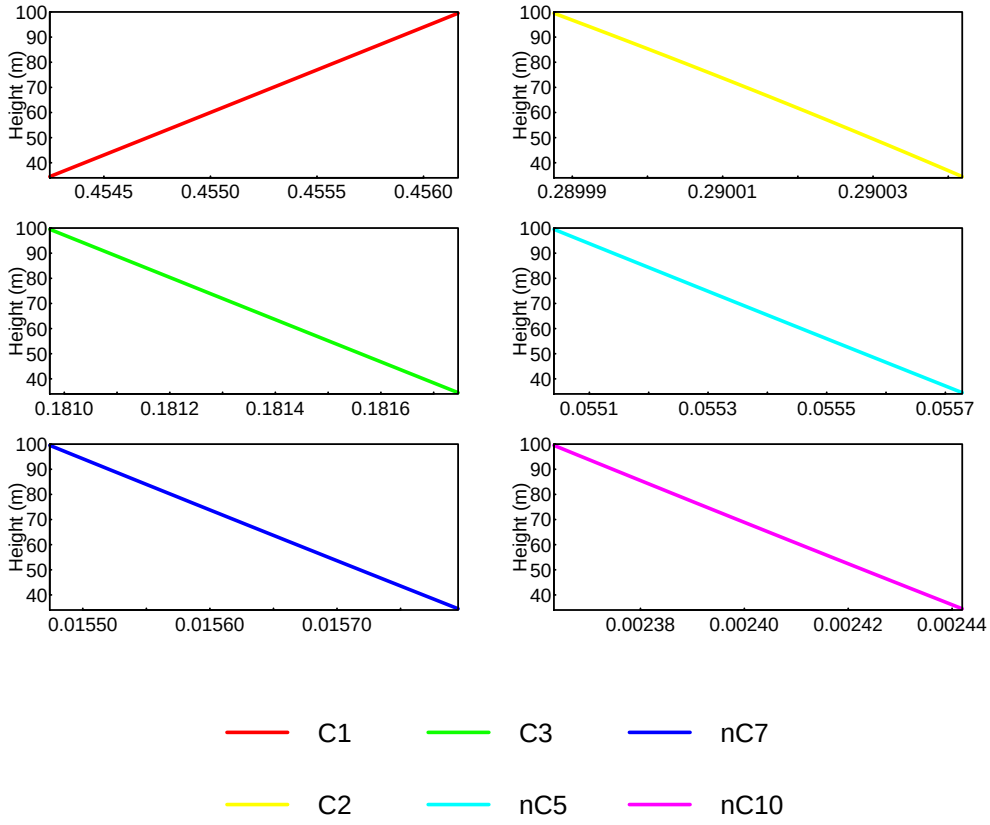

Figure 8: Compositional variance of C_1, C_2, C_3, nC_5, nC_7 and nC_{10} in vapor phase.

As shown in Figure 9, there is a segment with small slope near the vapor-liquid interface. This is a numerical artifact resulting from the finite number of intervals along height direction. Figure 10 shows compositional gradients of all six components in the liquid phase when the number of height intervals is equal to 1000. It is clear the numerical artifact disappears with large number of height intervals.

Figure 11 presents the relative energy ratio, which is the ratio of the total energy at current time step to the total energy at initial time step, changes in the process of simulation. It is clear the total energy decreases with time steps.

At the first few steps, no phase splits so that energy decreases little. When two phases start to be generated, energy decays very quickly, resulting into high gradients in the middle, until it reaches the true equilibrium state.

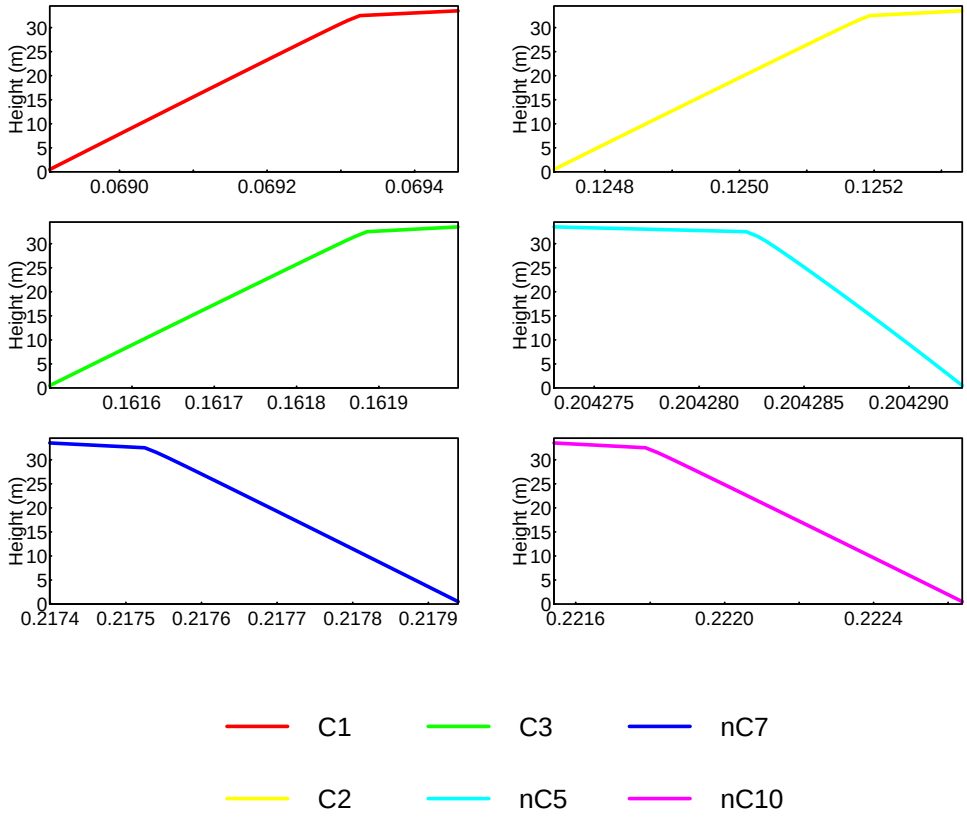

Figure 9: Compositional variance of C_1, C_2, C_3, nC_5, nC_7 and nC_{10} in liquid phase.

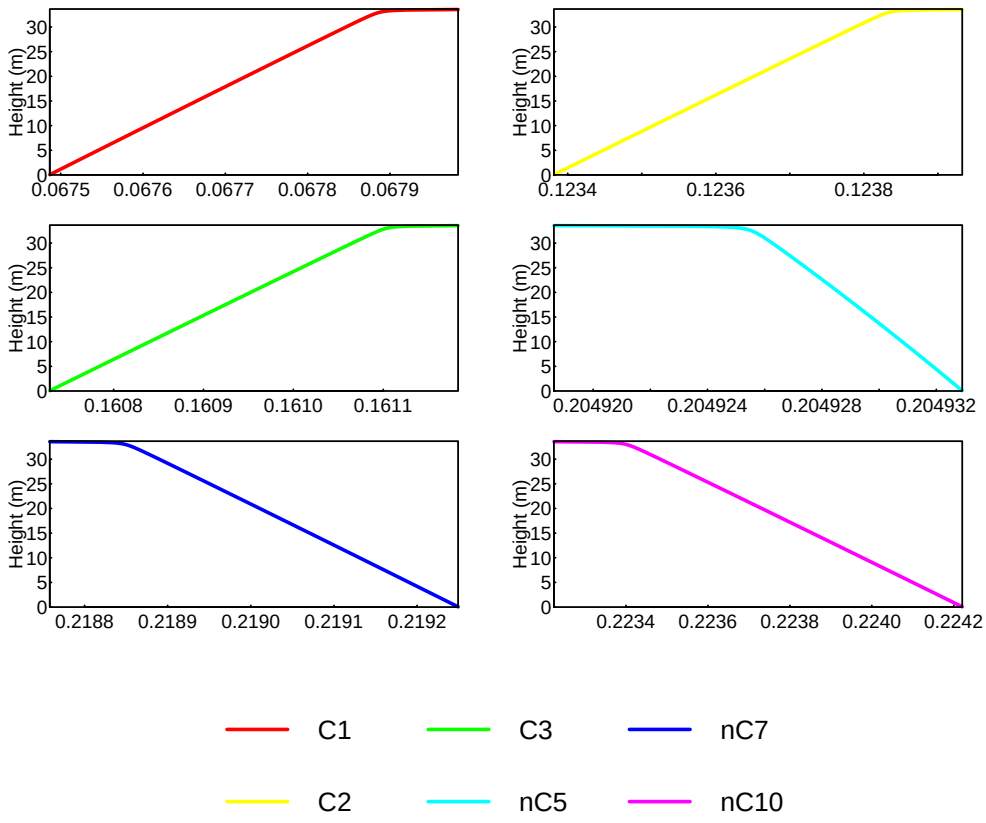

Figure 10: Compositional variance of C_1, C_2, C_3, nC_5, nC_7 and nC_{10} in liquid phase for 1000 intervals.

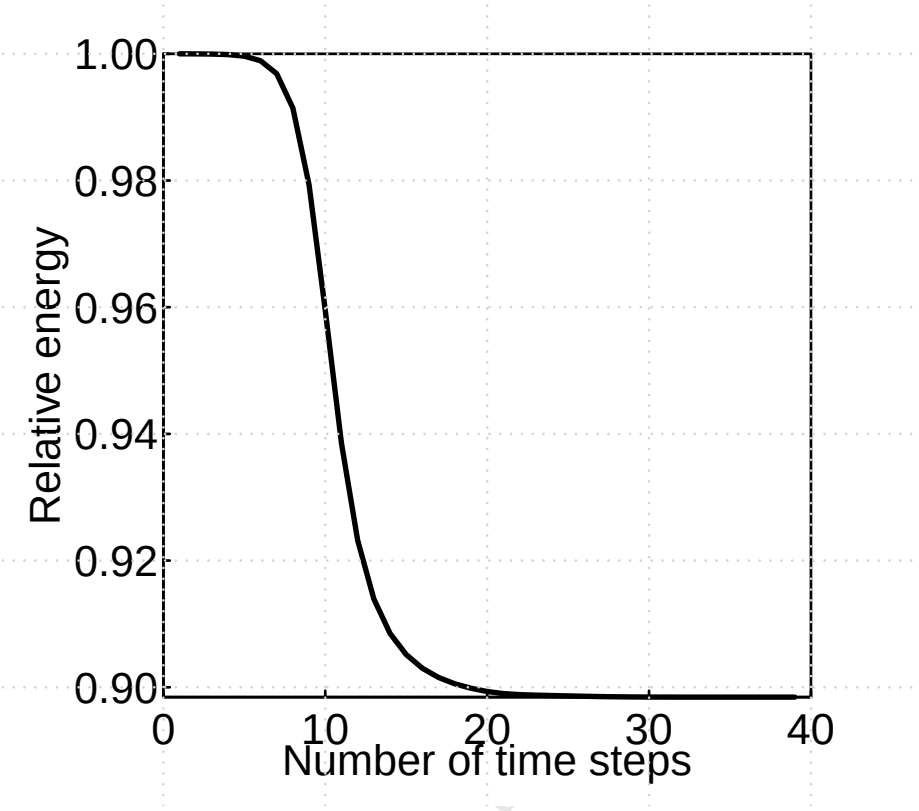

Figure 11: Relative energy change from non-equilibrium state to equilibrium state at 378.15 K.

5 Conclusions

In this paper, we derive an isothermal compositional grading model by minimizing the total energy and incorporating Lagrange multipliers for mass conservation. A semi-implicit convex splitting method is proposed to construct a unconditionally stable time marching scheme. The convex parts of Helmholtz free energy density and its derivative must be treated implicitly and the concave parts must be treated explicitly so that energy unconditionally dissipates with time. By this method, a system of transient equations is generated. With a good initial estimate of single-phase composition, it can help us efficiently calculate the compositional variance, automatically split the unstable single phase into two phases, determine the existence of gas-oil contact and locate the gas-oil contact if it exists. Unlike previous works, there is no need to do the stability analysis at each depth and save us a lot of time to search the gas-oil contact.

Appendix

For a mixture composed of N components, we denote by n_i the molar density of component i, and let $\mathbf{n} = (n_1, n_2, \ldots, n_N)^T$ and $n = n_1 + n_2 + \ldots + n_N$. The total energy is the sum of two contributions: the Helmholtz free energy f_h at local composition $\mathbf{n}$, and the gravitational potential energy f_g

$$F(\mathbf{n}) = \int_\Omega (f_h(\mathbf{n}) + f_g)\,\mathrm{d}x, \tag{1}$$

where Ω is a spatial domain. Denote by $M_{w,i}$ the molecualr weight of component i, and then the mass density of the mixture is expressed as

$$m = \sum_{i=1}^{N} M_{w,i} n_i.$$

The gravational potential energy f_g has the form

$$f_g = mgh, \tag{2}$$

where g is the absolute value of the gravity acceleration and h is the height relative to its being on the bottom of Ω. Denote by H the maximum height of the domain Ω, and then $h \in [0, H]$. The Helmholtz free energy $f_h(\mathbf{n})$ of a Peng-Robinson fluid is given by

$$f_h(\mathbf{n}) = f_h^{\text{ideal}}(\mathbf{n}) + f_h^{\text{excess}}(\mathbf{n}), \tag{3}$$

$$f_h^{\text{ideal}}(\mathbf{n}) = RT \sum_{i=1}^{N} n_i(\ln n_i - 1), \tag{4}$$

$$f_h^{\text{excess}}(\mathbf{n}) = -nRT\ln(1 - bn) + \frac{a(T)n}{2\sqrt{2}b} \ln\left(\frac{1 + (1 - \sqrt{2})bn}{1 + (1 + \sqrt{2})bn}\right), \tag{5}$$

where T is the temperature of the mixture and R is the universal gas constant. Here, b is the co-volume parameter and $a(T)$ is the energy parameter. For a mixture, these parameters are related to the ones of the pure fluids by mixing rules.

We now describe the computations of parameters $a(T)$ and b in (5). Let P be the pressure of mixture and let T_{c_i}, P_{c_i} and ω_i be critical temperature, critical pressure and acentric factor, respectively, of component i. For each component, we define the reduced pressure as $P_{r_i} = P/P_{c_i}$ and the reduced temperature as $T_{r_i} = T/T_{c_i}$, and furthermore, we define the mole fraction $x_i = n_i/n$. Then $a(T)$ and b are calculated by

$$a(T) = \sum_{i=1}^{N}\sum_{j=1}^{N} x_i x_j (a_i a_j)^{1/2}(1 - k_{ij}), \quad b = \sum_{i=1}^{N} x_i b_i, \tag{6}$$

where

$$a_i = 0.45724 \frac{R^2 T_{c_i}^2}{P_{c_i}} \left[1 + m_i\left(1 - \sqrt{T_{r_i}}\right)\right]^2, \quad b_i = 0.07780 \frac{RT_{c_i}}{P_{c_i}}. \tag{7}$$

In addition, k_{ij} is the given binary interaction coefficients for the energy parameters. The coefficient m_i is function of the acentric factor ω_i as

$$m_i = 0.37464 + 1.54226\omega_i - 0.26992\omega_i^2, \quad \omega_i \leq 0.49, \tag{8}$$

$$m_i = 0.379642 + 1.485030\omega_i - 0.164423\omega_i^2 + 0.016666\omega_i^3, \quad \omega_i > 0.49, \tag{9}$$

with

$$\omega_i = \frac{3}{7}\left(\frac{\log 10\left(\frac{P_{c,i}}{1\,\mathrm{atm}}\right)}{\frac{T_{c_i}}{T_{b_i}} - 1}\right) - 1, \tag{10}$$

where T_{b_i} is the normal boiling temperature of component i.

The above Peng-Robinson equation of state (PR-EOS) (Peng and Robinson, 1976) is selected both to model the homogeneous fluid and to derive an expression for the Helmholtz free energy density required in the gradient theory. The PVT function of PR-EOS has the following form:

$$P = \frac{RT}{v-b} - \frac{a(T)}{v(v+b)+b(v-b)}, \tag{11}$$

where v is the molar volume of mixtures. By the relation $n = 1/v$, we have

$$P = \frac{nRT}{1-bn} - \frac{n^2 a(T)}{1+2bn-b^2n^2}. \tag{12}$$

We note that (3)-(5) are consistent with (12). The chemical potential μ_i of component i is defined by

$$\left(\frac{\partial f_h(\mathbf{n})}{\partial n_i}\right)_{T,n_{\neq i}}, \tag{13}$$

where $n_i = (n_1, n_2, \ldots, n_{i-1}, n_{i+1}, \ldots, n_N)^T$.

Acknowledgment

This work is supported by the KAUST research fund awarded to the Computational Transport Phenomena Laboratory at KAUST.

References

Cahn, J. and Allen, S. (1977). A microscopic theory for domain wall motion and its experimental verification in Fe-Al alloy domain growth kinetics. *Le Journal de Physique Colloques*, (3):51–54.

Cai, J., Ghanbarian, B., Xu, P., Elsworth, D., Wang, M., Zhang, Z., and Wood, D. (2017). Virtual special issue: Advanced theoretical and numerical approaches and applications to enhanced gas recovery. *Journal of Natural Gas Science and Engineering*, 37:579–583.

Fan, X., Kou, J., Qiao, Z., and Sun, S. (2017). A componentwise convex splitting scheme for diffuse interface models with van der waals and peng–robinson equations of state. *SIAM Journal on Scientific Computing*, 39(1):B1–B28.

Firoozabadi, A. (2015). *Thermodynamics and Applications of Hydrocarbon Energy Production*. McGraw Hill Professional.

Galliero, G., Montel, F., et al. (2009). Understanding compositional grading in petroleum reservoirs thanks to molecular simulations. In *EUROPEC/EAGE Conference and Exhibition*. Society of Petroleum Engineers.

Halldórsson, S. and Stenby, E. H. (2000). Isothermal gravitational segregation: Algorithms and specifications. *Fluid Phase Equilibria*, 175(1-2):175–183.

Høier, L. and Whitson, C. H. (2001). Compositional Grading—Theory and Practice. *SPE Reservoir Evaluation & Engineering*, 4(06):525–535.

Kord, S. and Zobeidi, K. (2007). Effect of Compositional Grading on Reservoir Fluid Characterization in a Giant Iranian Oil Reservoir. In *Canadian International Petroleum Conference*, page 6.

Kou, J. and Sun, S. (2015). Numerical methods for a multicomponent two-phase interface model with geometric mean influence parameters. *SIAM Journal on Scientific Computing*, 37(4):B543–B569.

Kou, J. and Sun, S. (2016). Multi-scale diffuse interface modeling of multi-component two-phase flow with partial miscibility. *Journal of Computational Physics*, 318:349–372.

Kou, J. and Sun, S. (2017). Efficient energy-stable dynamic modeling of compositional grading. *International Journal of Numerical Analysis and Modeling*, 14(2):218–242.

Kou, J., Sun, S., and Wang, X. (2016). An energy stable evolution method for simulating two-phase equilibria of multi-component fluids at constant moles, volume and temperature. *Computational Geosciences*, 20(1):283–295.

Mokhtari, R. and Ashoori, S. (2013). Importance of Compositional Grading in Reservoir Development Studies; a Case Study. *J. Sci. Int. (Lahore)*, 25(3):457–459.

Montel, F., Gouel, P., et al. (1985). Prediction of compositional grading in a reservoir fluid column. In *SPE Annual Technical Conference and Exhibition*. Society of Petroleum Engineers.

Peng, D.-Y. and Robinson, D. B. (1976). A New Two-Constant Equation of State. *Industrial & Engineering Chemistry Fundamentals*, 15(1):59–64.

Ratulowski, J., Fuex, A., Westrich, J., Sieler, J., et al. (2000). Theoretical and experimental investigation of isothermal compositional grading. In *SPE Annual Technical Conference and Exhibition*. Society of Petroleum Engineers.

Sage, B. H., Lacey, W. N., et al. (1939). Gravitational concentration gradients in static columns of hydrocarbon fluids. *Transactions of the AIME*, 132(01):120–131.

Schulte, A. (1980). Compositional Variations Within a Hydrocarbon Column Due To Gravity. *Proceedings of SPE Annual Technical Conference and Exhibition*, (1).

Struwe, M. (2008). *Variational Methods: Applications to Nonlinear Partial Differential Equations and Hamiltonian Systems*. Springer-Verlag Berlin Heidelberg.

Sun, S. and Wheeler, M. F. (2005). Symmetric and Nonsymmetric Discontinuous Galerkin Methods for Reactive Transport in Porous Media. *SIAM Journal on Numerical Analysis*, 43(1):195–219.

Sun, S. and Wheeler, M. F. (2006). Anisotropic and dynamic mesh adaptation for discontinuous Galerkin methods applied to reactive transport. *Computer Methods in Applied Mechanics and Engineering*, 195(25-28):3382–3405.

Sun, S. and Wheeler, M. F. (2007). Discontinuous Galerkin methods for simulating bioreactive transport of viruses in porous media. *Advances in Water Resources*, 30(6-7):1696–1710.

Ting, P. D., Dindoruk, B., Ratulowski, J., et al. (2009). Numerical investigation of gravitational compositional grading in hydrocarbon reservoirs using centrifuge data. *SPE Reservoir Evaluation & Engineering*, 12(05):793–802.

Union Gas Limited. (2017). Chemical Composition of Natural Gas. `https://www.uniongas.com/about-us/about-natural-gas/chemical-composition-of-natural-gas`. (accessed 17.02.20).

Whitson, C. H. and Belery, P. (1994). Compositional Gradients in Petroleum Reservoirs. *University of Tulsa Centennial Petroleum Engineering Symposium*, pages 443–459.

Zhonghua Qiao and Shuyu Sun (2014). Two-Phase Fluid Simulation Using a Diffuse Interface Model with Peng–Robinson Equation of State. *SIAM Journal on Scientific Computing*, 36(4):B708–B728.

- Systematic and rigorous derivation of isothermal compositional grading framework is established by minimizing total free energy and employing the variational principle.
- An unconditionally energy-stable algorithm is established using a special semi-implicit convex splitting method.
- The proposed method converges to the solution with satisfactory accuracy if a good initial estimate of mole compositions is provided.
- The proposed method automatically generates phase splitting.